Numerical simulation of turbulent sediment transport

O. Durán [1], B. Andreotti [2], P. Claudin [2]

1. Laboratoire de Physique et Mécanique des Milieux Hétérogènes (PMMH), UMR 7636 CNRS ESPCI - Univ. Paris Diderot - Univ. P.M. Curie, 10 Rue Vauquelin, 75005 Paris, France – philippe.claudin@espci.fr
2. Department of Geological Sciences, Univ. North Carolina, 104 South Rd. Mitchell Hall, Campus Box 3315, Chapel Hill, North Carolina 27515, USA

Abstract

Sediment transport is studied by means of two phase numerical simulations based on a discrete element method for particles coupled to a continuum Reynolds averaged description of hydrodynamics.. We analyse the mechanisms at the grain scale in the case of bed load, in order to give support to empirical transport laws. The vertical velocities of the grains are small and sediment transport occurs in a thin layer at the surface of the static bed. Steady, or `saturated' transport is reached when the fluid borne shear stress at the interface between the mobile grains and the static grains is reduced to its threshold value. The number of grains transported per unit surface is therefore limited by the flux of horizontal momentum towards the surface. However, the fluid velocity in the transport layer remains almost undisturbed so that the mean grain velocity scales with the fluid shear velocity u_*, eventually leading to a sediment flux scaling with the third power of u_*. The influence of the grain to fluid density ratio is systematically studied to reveal the transition between sub-aqueous bedload and aeolian saltation, for which the transport law has a different scaling with u_*. Based on the mechanisms identified in the steady case, we discuss the transient of saturation of sediment transport and in particular the saturation time and length. Finally, we investigate the exchange of particles between the mobile and static phases and we determine the exchange time of particles.

1. INTRODUCTION

Despite a wide literature, some fundamental aspects of sediment transport in turbulent flows are still only partly understood. In particular, derivations of transport laws, relating the sediment flux to the flow velocity, have a strong empirical or semi-empirical basis (see e.g. among many others Meyer-Peter and Muller (1948), Ribberink (1998), Camemen and Larson (2005), Greeley et al. (1996), Iversen and Rasmussen (1999), Kok and Renno (2009) and references therein), thus lacking more physics-related inputs. Also, the dynamical mechanisms limiting sediment transport, in particular the role of the bed disorder (Charru, 2006) and turbulent fluctuations (Marchioli et al., 2006; Baas, 2008; Le Louvetel-Poilly et al., 2009), remain matter of discussion.

Here we investigate the properties of steady homogeneous sediment transport using a novel numerical description of particle-laden flows, using two-phase numerical simulations based on a discrete element method for particles coupled to a continuum Reynolds averaged description of hydrodynamics. In particular, we examine the transition from bed-load to saltation by studying the influence of the grain to fluid density ratio ρ_p / ρ_f. A similar approach has recently been used to study the onset of aeolian saltation (Carneiro et al., 2011). The present paper summarizes the MARID presentation. More details on this work, as well as a more developed bibliography on the subject, can be found in Durán et al. (2012).

2. THE MODEL

The idea is to use a continuum description of hydrodynamics, averaged at a scale larger than the grain size. This means that the feedback of the particles on the flow is treated in the mean field manner. This method allows us to perform very long numerical simulations (typically $1000\sqrt{d/g}$), using a (quasi) 2D large spatial domain (typically 15000 spherical grains in a xyz box of respective dimensions $1000d \times 1d \times 1000d$), while keeping the complexity of the granular phase. Periodic boundary conditions are used in the x (flow) direction. We will now detail the different ingredients of the model - see table 1 for notations.

General:	length l	d
	acceleration	g
	time t	$\sqrt{d/g}$
	velocity v	$\sqrt{gd}$
Particles:	angular velocity ω	$\sqrt{g/d}$
	mass m	$\frac{\pi}{6}\rho_p d^3$
	moment of inertia I	md^2
	force f	mg
	contact stiffness k	mg/d
	damping constant γ	$m\sqrt{g/d}$
Fluid:	shear stress τ	$(\rho_p - \rho_f)gd$

Table 1: Units used in the model, expressed in terms of the grain density (ρ_p), the fluid density (ρ_f), the gravity (g) and the mean grain diameter (d).

2.1 Forces on particles

The grains have a spherical shape and are described by their position vector $\vec{r}$, velocity $\vec{u}$ and angular velocity $\vec{\omega}$. A given grain labelled p inside a fluid obeys the equations of motion,

$$m\frac{d\vec{u}^p}{dt} = m\vec{g} + \sum_q \vec{f}^{p,q} + \vec{f}^p_{fluid}$$

$$I\frac{d\vec{\omega}^p}{dt} = \frac{d}{2}\sum_q \vec{n}^{p,q} \times \vec{f}^{p,q} \tag{1}$$

where $\vec{g}$ is the gravity acceleration, $I = md^2/10$ is the moment of inertia of a sphere, $\vec{f}^{p,q}$ is the contact force with grain q, $\vec{n}^{p,q}$ is the contact direction, and $\vec{f}^p_{fluid}$ encodes forces of hydrodynamical origin.

We model the contact forces following a standard approach for the modeling of contact forces in MD codes (see e.g. DEM book (2011) and references therein), where normal and tangential components are described by spring dash-pot elements. A microscopic friction coefficient is also introduced. For simplicity we assume that the net hydrodynamical force ($\vec{f}^p_{fluid}$) acting on a grain p due to the presence of the fluid is dominated by the drag and Archimedes forces, $\vec{f}^p_{drag}$ and $\vec{f}^p_{Arch}$, respectively. The lift force, lubrication forces and

the corrections to the drag force (Basset, added-mass, Magnus, etc.) are neglected.

Drag force — We hypothesize here that the drag force exerted by a homogeneous fluid on a moving grain only depends on the difference between the grain velocity $\vec{u}^p(x,z)$ and the fluid velocity $\vec{u}(z)$ at grain's height z. Introducing the particle Reynolds number R_u based on this fluid-particle velocity difference $R_u = |\vec{u} - \vec{u}^p|\, d/v$, the drag force can be written under the form

$$\vec{f}^p_{drag} = \frac{\pi}{8}\rho_f d^2 C_d(R_u)\,|\vec{u} - \vec{u}^p|\,(\vec{u} - \vec{u}^p) \tag{2}$$

where $C_d(R_u)$ is the drag coefficient. We use the following convenient phenomenological approximation (Ferguson and Church, 2004): $C_d(R_u) = [\sqrt{C_d^\infty} + \sqrt{R_u^c/R_u}]^2$, where $C_d^\infty \approx 0.5$, is the drag coefficient of the grain in the turbulent limit ($R_u \to \infty$), and $R_u^c \approx 24$ is the transitional particle Reynolds number above which the drag coefficient becomes almost constant.

Archimedes force — This force results from the stress which would have been exerted on the grain, if the grain had been a fluid. Thus,

$$\vec{f}^p_{Arch} = \frac{\pi}{6}d^3 \, div\sigma^f \tag{3}$$

where $\pi d^3/6$ is the grain volume and $\sigma^f_{ij} = -p^f\delta_{ij} + \tau^f_{ij}$ is the undisturbed fluid stress tensor (written in terms of the pressure p^f and the shear stress tensor τ^f_{ij}). In first approximation, the stress is evaluated at the center of the grain.

2.2 Hydrodynamics and coupling

In the presence of particles occupying a volume fraction ϕ, the hydrodynamics is described by the two-phase flow Reynolds averaged Navier-Stokes equations:

$$\rho_f(1-\phi)D_t u_i = -\partial_i p^f + \rho_f(1-\phi)g_i + \partial_j \tau^f_{ij} - F_i \tag{4}$$

where $D_t u_i = \partial_t u_i + u_j\partial_j u_i$ denote the fluid inertia. τ^f_{ij} is the total shear stress tensor resulting both from viscous diffusion of momentum (viscous stress) and transport of momentum by turbulent fluctuations (Reynolds stress). $\vec{F}$ is the body force exerted by the grains on the fluid. In the steady and

homogeneous case investigated here, These RANS equations simplify into

$$\partial_z p^f = -\rho_f g \tag{5}$$

$$\partial_z \tau^f = F_x \tag{6}$$

where we note $\tau^f = \tau^f_{xz}$ the fluid shear stress, and later on $u = u_x$ for the fluid horizontal velocity.

The coupling term $\vec{F}$ can then be obtained by averaging the hydrodynamical force $\vec{f}^p_{fluid}$ acting on all the grains moving around altitude z, in a horizontal layer of area A and thickness dz:

$$\vec{F}(z) = \frac{1}{Adz} \left\langle \sum_{p \in \{z;z+dz\}} \vec{f}^p_{fluid} \right\rangle \tag{7}$$

We take for A the total horizontal extent of the domain (i.e. $1000d \times 1d$). The symbols $\langle . \rangle$ denote ensemble averaging. Here, we retain its x-component only, which simplifies into

$$F_x = \frac{\phi}{1-\phi} \left\langle \sum_{p \in \{z;z+dz\}} f^p_{drag,x} \right\rangle / \sum_{p \in \{z;z+dz\}} \frac{\pi}{6} d^3 \tag{8}$$

where the grain's volume fraction ϕ is defined as

$$\phi(z) = \frac{1}{Adz} \sum_{p \in \{z;z+dz\}} \frac{\pi}{6} d^3 \tag{9}$$

Eq 6 integrates as $\tau^f(z) = \rho_f u_*^2 - \tau^p(z)$, where we have introduced the shear velocity u_*, defined by the undisturbed (grain free) wall shear stress, and the grain borne shear stress τ^p, computed from the integration of (8) over sufficient vertical extension to count all moving grains.

In order to relate the fluid borne shear stress to the average fluid velocity field, we adopt a Prandtl-like turbulent closure. Introducing the turbulent mixing length ℓ, we write

$$\tau^f = \rho_f (v + \ell^2 |\partial_z u|) \partial_z u \tag{10}$$

v is the viscosity (a constant independent of the volume fraction). As for the mixing length ℓ, we know it should vanish below some critical Reynolds number R_c and should be equal to the distance to the surface z, far above the transport layer. To avoid the need of a somewhat arbitrary definition of an interface between he static and mobile zones of the bed, we propose the differential equation

$$v \partial_z \ell = \kappa \left| 1 - e^{\sqrt{\frac{1}{R_c}\left(\frac{u\ell}{v}\right)}} \right| \tag{11}$$

where $\kappa \approx 0.4$ is von Karman's constant. In the case of a turbulent flow over a smooth and flat surface (no grains), we recover the prediction computed with the phenomenological expression for the mixing length suggested by van Driest (Pope, 2000), which reproduces well classical experimental results. Comparison to measurements determines the dimensionless parameter $R_c \approx 7$.

Starting integration deep enough in the static bed to be in the asymptotic limit that can be analyticaly derived, we obtain the different hydrodynamical fields. They are displayed in Fig. 1, in the case of sub-aqueous transport ($\rho_p / \rho_f = 2$).
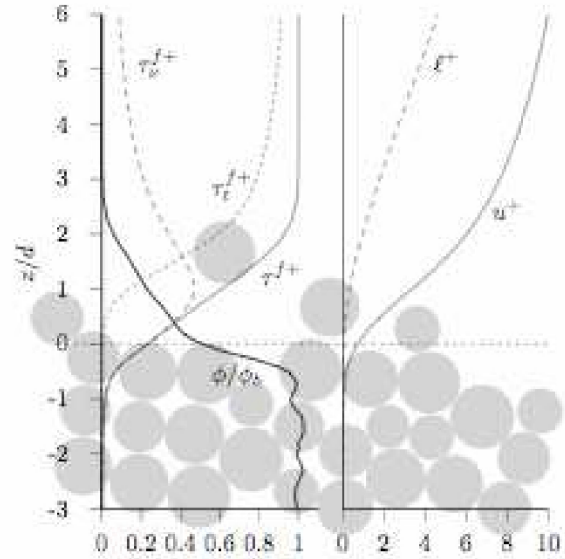

Figure 1. Vertical profiles of the rescaled volume fraction ϕ / ϕ_b, flow velocity $u^+ = u / u_*$, mixing length $\ell^+ = \ell / d$, fluid borne shear stress $\tau^{f+} = \tau^f / (\rho_f u_*^2)$, viscous shear stress $\tau^{f+}_v = v \partial_z u / u_*^2$ and turbulent shear stress $\tau^{f+}_t = (\ell \partial_z u)^2 / u_*^2$ (by definition $\tau^{f+} = \tau^{f+}_v + \tau^{f+}_t$). The reference height $z = 0$ is set at the altitude such that $\phi = \phi_b / 2$.

99

3. SEDIMENT FLUX

Steady and homogeneous sediment transport is quantified by the volumetric saturated flux q_{sat}, i.e. the volume of the particles (at the bed density) crossing a vertical surface of unit transverse size per unit time. It has the dimension of a squared length per unit time. In the simulations, we compute it as

$$q_{sat} = \frac{1}{A\phi_b}\frac{\pi}{6}d^3\sum_p u_p \qquad (12)$$

A key issue is the dependence of q_{sat} on the shear velocity or, equivalently, its dimensionless counterpart the Shields number Θ, defined by

$$\Theta = \frac{\rho_f u_*^2}{(\rho_p - \rho_f)gd} \qquad (13)$$

which encodes the strength of the flow.

Figure 2. Rescaled saturated flux versus $\Theta^{3/2}$ for water (a) and Θ for air (b). Full lines are the predictions given in the text.

We show in Fig. 2 the saturated flux in both cases (water and air). In agreement with experimental observations (e.g., Meyer-Peter and Muller, 1948; Ribberink, 1998; Lajeunesse et al., 2010; Rasmussen et al., 1996; Creyssels et al., 1009), we find that q_{sat} scales asymptotically as Θ (or u_*^2) for saltation, while q_{sat} scales as $\Theta^{3/2}$ (or u_*^3) underwater. This figure also reveals the existence of a threshold shear velocity below which the flux vanishes. More precisely, we define the dynamical threshold Shield number Θ_d from the extrapolation of the saturated flux curve to 0, which gives in our case $\Theta_d \approx 0.12$ for water ($\rho_p/\rho_f = 2$) and $\Theta_d \approx 0.004$ for air ($\rho_p/\rho_f = 2000$), respectively. These values are consistent with experimental ones within a factor of 2.

4. MECANISMS AT WORK IN THE TRANSPORT LAYER

Bed load and saltation mainly differ by the vertical characteristics of the transport layer. At small density ratios the motion of grains is confined within a thin layer of few grain diameters. By contrast, for large density ratios, grains experience much higher trajectories: the transport layer is much wider and the flux density decreases exponentially with height with a characteristic size of the order of $50d$, roughly independent of the shear velocity. The transport layer thickness is effectively determined by the hop length for $\rho_p/\rho_f > 10$. Below this cross-over value, this thickness is given by the grain diameter d, as trajectories are almost horizontal. The transition from bed load to saltation therefore takes place when the vertical velocities of the particles are sufficiently large for these particles to escape the traps formed by the grains on the static bed.

Another difference between bed load and saltation is how the grain's feedback on the flow is distributed within the steady state transport layer. Fig. 3 presents the vertical profiles of the fluid shear stress, rescaled by the dynamical threshold τ_d (as defined by the saturated flux), for different shear velocities. For bed load (Fig. 3a), the different profiles of the fluid shear stress seems to
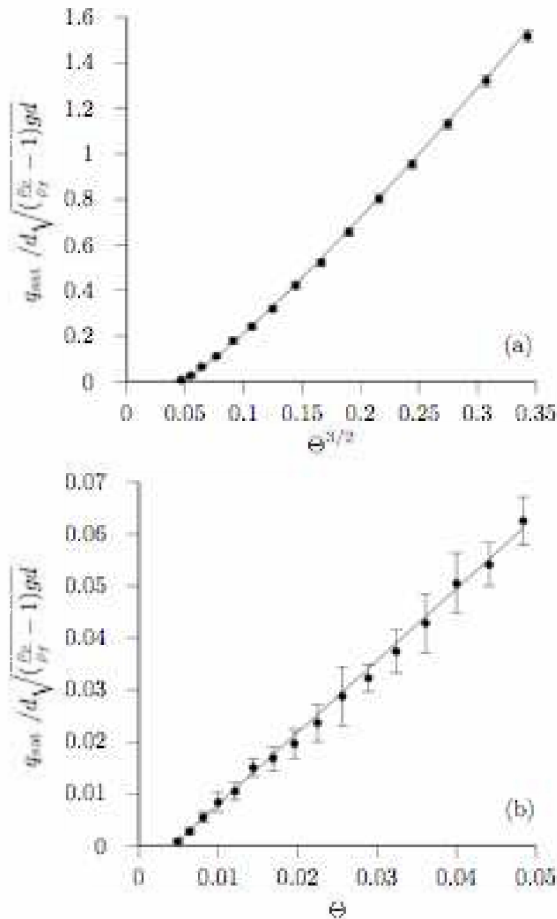
converge to the threshold value very close to the surface ($z = 0$). In this transport layer, the fluid momentum decays over few grain sizes, in agreement with the vertical extension of the transport layer. By contrast, the fluid shear stress is below the threshold in the bed ($z < 0$) but some (weak) transport still occurs there, which is sustained not by the fluid itself but by the momentum transferred to the surface by grain collisions.

This general picture is still valid for saltation (Fig. 3b), however now the dynamical threshold is reached much farther from the surface (at $z \approx 10d$) which implies that the kinetic energy of impacting grains is large enough as to sustain the transport below this height. Above it, the transport is driven by the fluid and most of its momentum is dissipated in a much larger layer (comprising tens of grain diameters) again in agreement with the size of the saltation layer. Notice that although this surface sublayer below $10d$ contains most of the grains, it still represents a small fraction of the overall transport layer.

An important consequence of this distinction in the vertical structure of the grain's feedback is that although for bed load transport is equilibrated when the fluid shear stress reaches its dynamical threshold below the transport layer, this condition is not enough for saltation to equilibrate. For saltation there is a sub-layer where transport is not directly driven by the fluid and thus its equilibration is not dictated by the threshold. There, the properties of grain's collisions become relevant and the equilibrium is described by the conservation of the number of saltating grains i.e. when the number of grains entering the flow exactly balance those grains trapped by the bed.

5. SCALING LAWS

The saturated flux can then be decomposed as the product of the number n of transported grains per unit area by the mean grain horizontal velocity $\overline{u}^P$: $q_{sat} = n\overline{u}^P \pi d^3 /(6\phi_b)$. In the numerical simulations, we compute n and $\overline{u}^P$ as

$$n = \frac{\left(\sum_p u_p\right)^2}{A\sum_p u_p^2} \quad \text{and} \quad \overline{u}^P = \frac{\sum_p u_p^2}{\sum_p u_p} \qquad (14)$$

These quantities are plotted as functions of the Schields number in Fig. 4. A scaling law $n \propto \Theta - \Theta_d$ is well verified over two decades, independently of ρ_p/ρ_f. By contrast, the density ratio has a strong effect of $\overline{u}^p$. The mean grain velocity is independent of Θ for large ρ_p/ρ_f (aeolian case), whereas it varies linearly with the fluid shear velocity at low density ratio (sub-aqueous case). Interestingly, $\overline{u}^p$ remains finite at the threshold, at a value independent of ρ_p/ρ_f. These behaviours are in agreement with experimental findings in the case of bedload (Lajeunesse et al., 2010).
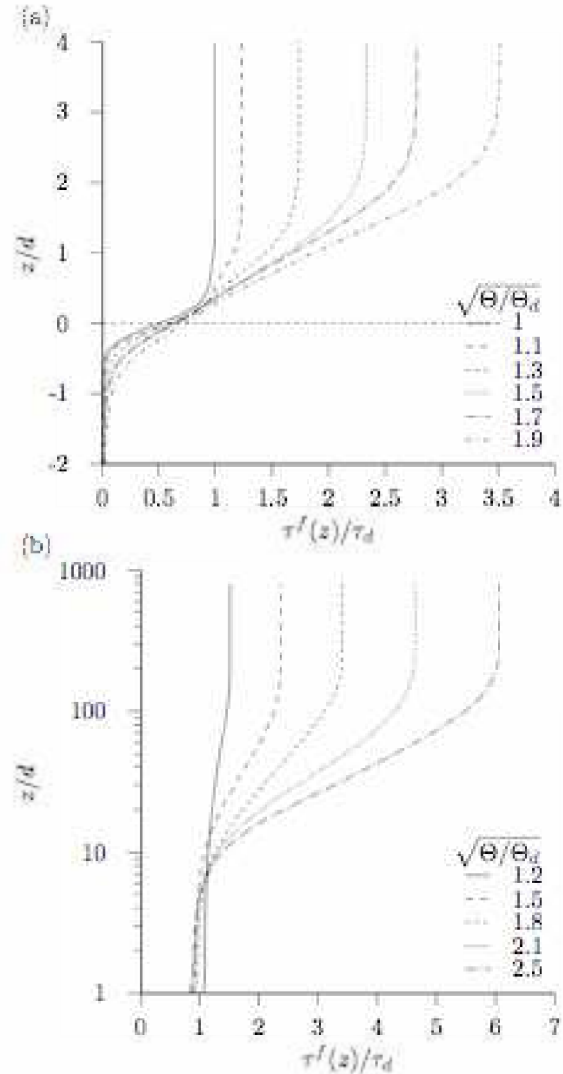

Figure 3. Vertical profiles of the fluid borne shear stress for different values of the shear velocity ratio (see legend), in water (a) and air (b).
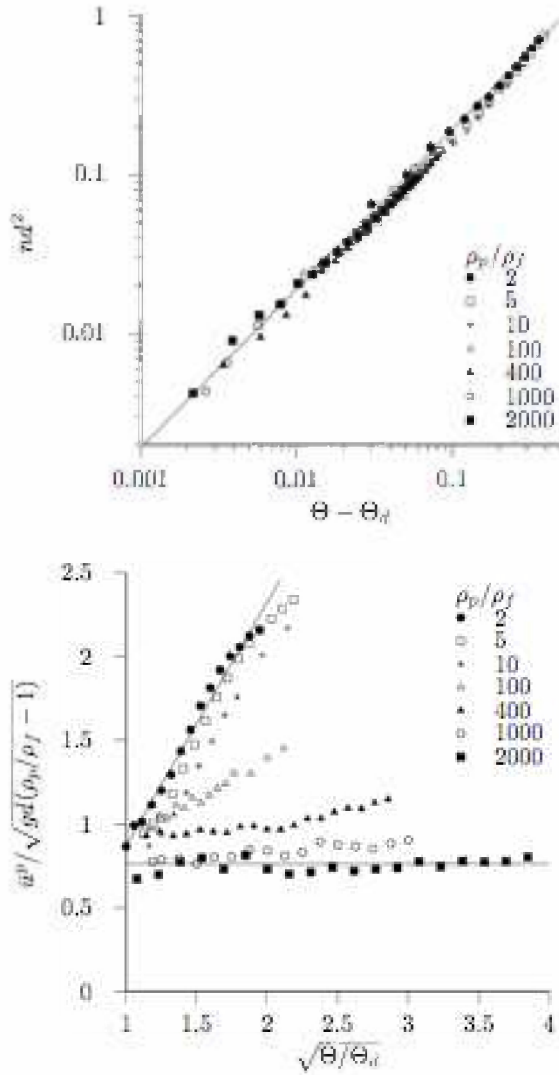
Figure 4. (a) Number of transported grains per unit area and (b) mean velocity of these grains as functions of the Shields number for different values of the density ratio (see legend).

We can derive these scaling laws from simple models. Following Bagnold's (1956) original ideas for the case of bedload, we write the grain born shear stress τ^p as proportional to the moving grain density n and to the drag force f_d acting on a moving grain. As these grains are in steady motion, f_d balances a resistive force due granular friction, collisions with the bed, etc. These different dissipative mechanisms can be modeled as an overall effective friction force characterized by a friction coefficient μ_d, leading to $f_d = \pi/6\mu_d(\rho_p - \rho_f)gd^3$. Saturation is reached

when the fluid shear stress equals the transport threshold at the surface of the static bed, i.e. when $\tau^p = \rho_f u_*^2 - \tau_d$, with, by definition, $\tau_d = \Theta_d(\rho_p - \rho_f)gd = \rho_f u_d^2$. As consequence, the number of transported particles per unit area is solely determined by the excess shear stress: $n = (\rho_f u_*^2 - \tau_d)/f_d$. Assuming that the transported grains do not disturb the flow, the flow velocity around grains u must be proportional to the shear velocity, so that $u/u_d = \sqrt{\Theta/\Theta_d}$. One can then deduce: $\bar{u}^p = u_d(\sqrt{\Theta/\Theta_d} - \sqrt{\mu_d/\mu_s})$, where μ_s is a friction coefficient characterising the drag force necessary to set into motion a static grain. This predicts that the grain velocity does not vanish at the threshold, if friction is lowered during motion ($\mu_d < \mu_s$). The velocity at threshold can be interpreted as the velocity needed by a grain to be extracted from the bed and entrained by the flow.

We can proceed in a similar manner for the aeolian saltation regime, following ideas initially proposed by Owen (1964) and Ungar and Haff (1987). The momentum balance $\tau^p = \rho_f u_*^2 - \tau_d$ still holds, so that n has the same form as in the bed-load case, but with a different effective drag force f_d, not related to friction anymore but to grain velocities. For saltation, steady transport also implies that the number of grains expelled from the bed into the flow exactly balances those trapped by the bed, i.e. a replacement capacity equal to one. Due to the grain feedback on the flow, in contrast with bed load, grains in the transport layer feel a flow independent of the wind strength (see Fig. 3). Thus, new moving grains come only from high energy bed collisions. Since the number of ejected grains is a function of the impact energy (or equivalently, of the impact velocity), the mean grain velocity $\bar{u}^p$ must be constant, independent of the shear velocity, scaling with u_d. In fact, all particle surface velocities also scale with u_d, so that f_d is a constant too, leading again to $n \propto \Theta - \Theta_d$.

These scaling laws explain the different behaviours of $q_{sat}(\Theta)$ in the sub-aqueous bedload and aeolian saltation cases, as shown in Fig. 2.

6. CONCLUSIONS

The aim of this paper was to present a novel numerical approach for sediment transport based on a discrete element method for particles coupled to a continuum Reynolds averaged description of hydrodynamics. We have studied the effect of the grain to fluid density ratio and showed that we can reproduce both (sub-aqueous) bed load at ρ_p / ρ_f close to unity, where transport occurs in a thin layer at the surface of the static bed, and (aeolian) saltation at large ρ_p / ρ_f, where the transport layer is wider and more dilute. Scaling laws for the density of moving grains, and for the average velocity of these grains, as functions of the Schields number are found in agreement with experiments, and support simple mechanisms at work in steady and homogeneous transport.

Further work will be focused on transient situations, in order to study the time and length scales encoding the relaxation properties of out-of-equilibrium transport. Also, it would be interesting to investigate the case of bimodal or more polydisperse grains (Houssais and Lajeunesse, 2012)

7. ACKNOWLEDGMENT

8. REFERENCES

Baas, A.C.W. 2008 Challenges in aeolian geomorphology: investigating aeolian streamers. Geomorphology 93, 3-16.

Bagnold, R.A. 1956 The flow of cohesionless grains in fluids. Phil. Trans. R. Soc. Lond. 249, 235-297.

Camemen, B. and Larson, M. 2005 A general formula for non-cohesive bed-load sediment transport. Esturarine Coastal 63, 249-260.

Carneiro, M.V., Pahtz, T., and Herrmann, H.J. 2011 Jump at the onset of saltation. Phys. Rev. Lett. 107, 098001.

Charru, F. 2006 Selection of the ripple length on a granular bed. Phys. Fluids 18, 121508.

Creyssels, M., Dupont, P., Ould el Moctar, A., Valance, A., Cantat, I., Jenkins, J.T., Pasini, J.M., Rasmussen, K.R. 2009 Saltating particles in a turbulent boundary layer: experiment and theory. J. Fluid Mech. 625, 47-74.

Discrete-element Modeling of Granular Materials. Edited by F. Radjai and F. Dubois, ISTE, Wiley, 2011.

Durán, O., Andreotti, B. and Claudin, P. 2012 Numerical simulation of turbulent sediment transport, from bed load to saltation. Phys. Fluids 24, 103306.

Ferguson, R.I. and Church, M. 2004 A simple universal equation for grain settling velocity, J. Sedim. Res. 74, 933-937.

Greeley, R., Blumberg, D.G. and Williams, S.H. 1996 Field measurement of the flux and speed of wind blown sand. Sedimentology 43, 41-52.

Houssais, M. and Lajeunesse, E. 2012 Bedload transport of a bimodal sediment bed. J. Geophys. Res. 117, F04015.

Iversen, J.D. and Rasmussen, K.R. 1999 The effect of wind speed and bed slope on sand transport. Sedimentology 46, 723-731.

Kok, J.F., Renno, N.O. 2009 A comprehensive numerical model of steady state saltation (COMSALT). J. Geophys. Res. 114, D17204.

Lajeunesse, E., Malverti, L. and Charru, F. 2010 Bedload transport in turbulent flow at the grain scale: experiments and modeling. J. Geophys. Res. 115, F04001.

Le Louvetel-Poilly, J., Bigillon, F., Doppler, D., Vinkovic, I., Champagne, J.-Y. 2009 Experimental investigation of ejections and sweeps involved in particle suspension. Water Resour. Res. 45, W02416.

Marchioli, C., Armenio, V., Salvetti, M.V. and Soldati, A. 2006 Mechanisms for deposition and resuspension of heavy particles in turbulent flow over wavy interfaces. Phys. Fluids 18, 025102.

Meyer-Peter, E. and Muller, R. 1948 Formulas for bed load transport. Proc., 2nd Meeting, IAHR, Stockholm, Sweden, 39-64.

Owen, P.R. 1964 Saltation of uniform grains in air. J. Fluid Mech. 20, 225-242.

Pope, S.B. 2000 Turbulent flows. Cambridge University Press.

Rasmussen, K.R., Iversen, J.D., Rautaheimo, P. 1996 Saltation and wind flow interaction in a variable slope wind tunnel. Geomorphology 17, 19-28.

Ribberink, J.S. 1998 Bed-load transport for steady flows and unsteady oscillatory flows. Coastal Eng. 34, 58-82.

Ungar, J.E. and Haff, P.K. 1987 Steady state saltation in air. Sedimentology 34, 289-299.